Heavy atom-free semiconducting polymer with high singlet oxygen quantum yield for prostate cancer synergistic phototherapy†

Jian Shen,[a] Jianjiao Chen,[b] Zhen Ke,[b] Dengfeng Zou, [ID][b] Liguo Sun*[a] and Jianhua Zou [ID] *[bc]

Photodynamic and photothermal synergistic therapy are newly developed approaches for cancer treatment. The design and preparation of photosensitizers of high phototoxicity as well as low dark toxicity are of increasing significance in minimizing the side effects and maximizing the phototherapy efficacy of such treatments. In this study, a heavy atom-free copolymer **NDNT** was designed and synthesized by the Stille coupling reaction. This compound shows a high singlet oxygen quantum yield of 55.2%, guaranteeing an excellent phototherapy efficacy. The nanoparticles (NPs) of **NDNT** obtained by nanoprecipitation with DSPE-PEG$_{2000}$ with an average diameter of 65 nm exhibit considerably high phototoxicity towards human prostate cancer cells (Du145) because their half inhibitory concentration (IC$_{50}$) is as low as 3.8 µg mL^{-1}. Simultaneously, the dark toxicity of the NPs is almost negligible, even at a high concentration. Furthermore, an *in vivo* study with laser irradiation by photodynamic and photothermal synergistic therapy demonstrates that the NPs are capable of inhibiting a Du145 tumor growth, compared with the control and dark group, suggesting the low dark toxicity and high phototoxicity of such NPs. The H&E stained pictures of the normal tissues show that no obvious damage occurred, indicating the biosafety of the **NDNT** NPs. These results provide a strategy for designing heavy atom-free copolymers for phototherapy both *in vitro* and *in vivo*.

Introduction

At present, malignant tumors have become the second leading cause for human death, and people in growing numbers are suffering from cancer worldwide, following heart disease.[1] Among the various cancers, prostate cancer is a universal challenge to man. Patients undergoing traditional cancer therapies, including surgery, radiation and chemotherapy, can have a higher possibility to suffer from side effects and a second recurrence of tumor.[2–6] Although surgery is aimed at completely removing the tumor as much as possible, the prostate is often closely adhered to the surrounding tissues, with the characteristic of invasive growth, and strong recurrence, thus leading to the difficulty in removing the tumor tissue completely.[5] Traditional drugs usually cause severe toxicity and side effects, and also lead to the condition of multiple drug resistance. Based on these observations, it is urgent to explore and discover effective treatment methods for such a common and serious disease.[7–10]

Phototherapy, including photodynamic therapy and photothermal therapy, is an invasive technique for tumor treatment.[11–19] Compared with traditional treatment methods, phototherapy has a therapeutic effect on a variety of tumors, does not produce drug resistance, and after long-term follow-up and evaluation. Furthermore, the photosensitizers can target the specific tumor site without causing damage to the surrounding normal tissues.[20–25]

Photosensitizers (PSs) play an important role in the phototherapy process. High phototoxicity as well as low dark toxicity may maximize the efficacy and simultaneously minimize the side effects. The high singlet oxygen quantum yield ($^1O_2$ QY) and photothermal conversion efficiency of PSs may promise an excellent therapy efficacy.[26] Heavy atoms are often conjugated to the molecule to enhance the $^1O_2$ QY *via* spin orbit crossing (SOC), but they may contribute to the dark toxicity of the PS itself. Heavy atom-free PS may lower the potential of dark toxicity, the design and preparation of which is of tremendous interest. PS with near infrared region (NIR) may have better penetration depth.[27–30]
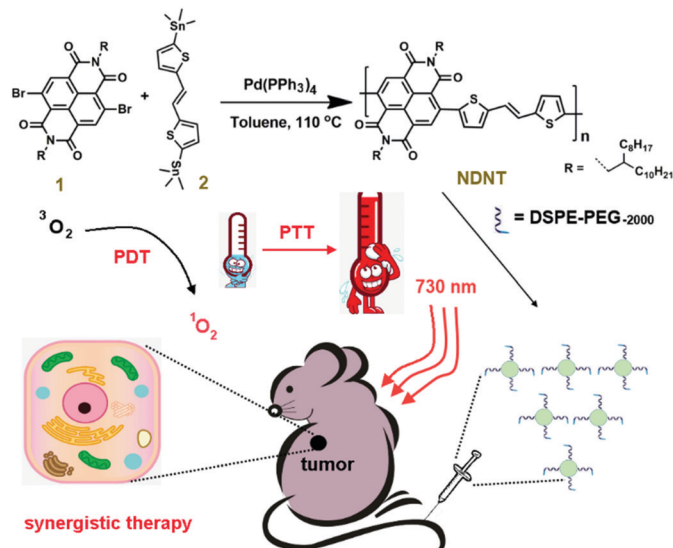
In this study, a heavy atom-free copolymer was prepared by the Stille coupling reaction for cancer therapy (Scheme 1).

[a] *Department of Urology, Changshu No. 2 People's Hospital, 215500, Jiangsu, P. R. China. E-mail: 13338729262@163.com*

[b] *School of Pharmacy, Guilin Medical University, Guilin 541004, Guangxi, P. R. China. E-mail: zoujh93@126.com*

[c] *Jiangsu Laboratory of Advanced Materials, Department of Chemistry and Materials Engineering, Changshu Institute of Technology, Changshu, 215500, Jiangsu, P. R. China*

† Electronic supplementary information (ESI) available. See DOI: 10.1039/c9qm00158a

This journal is © The Royal Society of Chemistry and the Chinese Chemical Society 2019

Mater. Chem. Front., 2019, **3**, 1123–1127 | 1123

Scheme 1 Synthesis of **NDNT** and illustration of its NPs for phototherapy.

The as-obtained **NDNT** with NIR absorbance (730 nm) has a high $^1O_2$ QY of 55.2%, with methylene blue as a standard substance in DCM. Nanoprecipitation was used to prepare the water soluble NPs with average diameter of 65 nm, which were suitable for *in vitro* and *in vivo* study. An MTT assay shows that **NDNT** NPs have an ultralow half inhibitory concentration (IC_{50}) of 3.8 μg mL^{-1} and a negligible dark toxicity even at high concentrations. An *in vivo* study demonstrates that **NDNT** NPs can effectively inhibit the tumor growth, while the normal tissues, including the spleen, liver, kidney, heart and lung, suffer from no damage. Our results suggest that **NDNT** NPs are a potential candidate for phototherapy.

Experimental

Materials and apparatus

Except for **NDNT**, all the chemicals were commercially purchased from Sigma and were used without further purification. ^{1}H NMR and ^{13}C NMR spectra were recorded on a Bruker DRX NMR spectrometer in CDCl$_3$ at 298 K with residual solvent (CDCl$_3$, δ = 7.26 ppm) as the internal standard. UV-vis spectra were recorded on a spectrophotometer (UV-3600 UV-Vis-NIR, Shimadzu, Japan). Fluorescence spectra were recorded on an F-4600 spectrometer (HITACHI, Japan). TEM images of the nanoparticles were recorded on a JEOL JEM-2100 equipment. DLS was measured on a 90 Plus particle size analyzer (Brookhaven Instruments, USA).

Synthesis and characterization of NDNT

Compound **1** (98.50 mg, 0.1 mmol) and compound **2** (51.80 mg, 0.1 mmol) were dissolved in anhydrous toluene (5 mL), to which Pd (PPh$_3$)$_4$ (4.65 mg, 0.004 mmol) was added. The solution mixture was stirred at 110 °C for 16 h under an argon atmosphere. After cooling to ambient temperature, the reaction mixture was poured into methanol (200 mL). The isolated crude product was then subjected to Soxhlet extraction with methanol,

hexane and acetone. Finally, the product was extracted with chloroform, which was concentrated before being precipitated with methanol again, affording a dark solid. Yield: 158 mg, 78%. δH (400 MHz, CDCl$_3$): 8.80–8.50 (2 H, br), 7.26–7.15 (2 H, br), 7.14–6.99 (4 H, br), 4.18–4.10 (4 H, br), 2.12–1.97 (2 H, br), 1.50–1.16 (64 H, br), 0.90–0.80 (12 H, br). M_w/M_n (GPC) 50.8k/31.4k. T_d (TGA) = 438 °C.

Preparation of the NDNT nanoparticles

The nanoparticles of **NDNT** were prepared by nanoprecipitation with DSPE-PEG$_{-2000}$. DSPE-PEG$_{-2000}$ (5 mg) was first dissolved in distilled water using ultrasound. Then, **NDNT** (5 mg) was dissolved in tetrahydrofuran (THF, 1 mL) and 200 μL of the **NDNT** solution was injected into PBS with ultrasound at room temperature. After the mixture was stirred for 10 min, the THF was removed by purging the solution with nitrogen. The product was then frozen and dried for further use.

Cell culture and MTT assay

At 37 °C, human prostate cancer Du145 cell lines were cultured in a medium made up of Dulbecco's modified Eagle's medium (DMEM, Gibco) with 10% fetal bovine serum (FBS) under an atmosphere of 5% CO$_2$. **NDNT** NPs were first dissolved in distilled water, which were then diluted with DMEM to various concentrations (0–6 μg mL^{-1}) and put into a 96-well plate. Then, the plate was irradiated with a laser (730 nm, 1 W cm^{-2}) for 5 minutes. The relative cell viability was determined using a MTT (3-(4,5-dimethylthiazol-2-yl)-2,5-diphenyltetrazolium bromide) assay. The MTT solution in distilled water (5 mg mL^{-1}, 20 μL) was added to each well followed by incubation for 4 h under the same conditions at 37 °C. The solution was then discarded, followed by the addition of DMSO (200 μL) to each well. At ambient temperature, the absorbance was measured on a Bio-Tek microplate reader. The cell viability of the control group was considered to be 100%. The relative cell viability was then calculated by the following equation: viability (%) = mean absorbance of the group incubated with **NDNT** NPs/mean absorbance of the group incubated with DMEM.

In vitro cellular uptake and fluorescence image of cellular ROS

Du145 cells were incubated with DSPE-PEG$_{-2000}$-coated **NDNT** NPs (3.8 μg mL^{-1}, 2 mL) in a confocal dish for different time in the dark over 24 h. Then, the solution was discarded and the cells were washed with PBS three times (1 mL), and then 1 mL polyoxymethylene was added for 25 min. Subsequently, the polyoxymethylene was discarded and the cells were washed with PBS (1 mL) for three times. The sample that had been incubated for 24 h with **NDNT** NPs was further cultured with 2,7-dichlorodihydrofluorescein diacetate (DCF-DA, 10 μmol) for 5 min. Following this, the dish was washed with PBS (1 mL) three times. This sample was irradiated with a laser for 3 minutes (730 nm, 1 W cm^{-2}). The samples that had not been incubated with **NDNT** NPs for 24 h were excited at the wavelength of 633 nm and the resultant fluorescence from 650 to 750 nm measured. The *in vitro* ROS generation was excited with a 488 nm laser and fluorescence from 490 to 600 nm was measured.

In vivo tumor treatment histology examination

The study complies with all institutional, national guidelines and National Institutes of Health. The protocol was approved by the Animal Center of Guilin Medical University (SCXK2007-001). 15 nude mice were purchased and then injected with Du145 cells into the armpit as the tumor source. These mice were then randomly divided into 3 groups randomly when the tumor volume reached about 100 mm^3. For the control group, the mice were intravenously injected with a saline solution, while the other groups were injected with **NDNT** NPs (38 μg mL^{-1}, 100 μL) in saline solution. After 4 h, the tumors of certain mice were irradiated by a laser (730 nm, 1 W cm^{-2}) for 8 minutes, while the other group of mice were not irradiated. The experiment was continued for 28 days, and the tumor volume and body weight of the mice were recorded every two days. These nude mice were sacrificed followed by the histology analysis. The main organs (heart, liver, spleen, lung, kidney) and the tumor was isolated and fixed in 4% formaldehyde solution. After dehydration, they were embedded in paraffin cassettes and stained with hematoxylin and eosin (H&E), and the images were recorded on a microscope.

Results and discussion

Synthesis and characterization of NDTT and NPs

As shown in Fig. 1A, **NDNT** NPs exhibited broad absorption peaks at 730 and 822 nm, while **NDNT** in DCM shows absorption with maximum intensity at 720 nm. For the emission spectra, **NDNT** shows emission with maximum intensity at 732 nm (Fig. 1B), while emission with a red shift of 36 nm was found for its nanoparticles. **NDNT** shows emission with a maximum intensity at 768 nm. The red-shift of 10 nm is caused by aggregation in water.

Then, the morphology and diameter of the nanoparticles were characterized using transmission electron microscope (TEM) and dynamic light scattering (DLS).

High singlet oxygen quantum yield ($^1O_2$ QY) promises excellent phototoxicity for a photosensitizer. The $^1O_2$ QY was determined using 1,3-diphenylisobenzofuran (DPBF) as a probe with methylene blue (MB) as a standard in DCM. As shown in Fig. 1C and D, the absorbance of DPBF degrades at a high speed with laser irradiation, and the $^1O_2$ QY calculated is as high as 55.2%. It is worth pointing out that the copolymer is heavy atom-free but possesses a high $^1O_2$ QY, which may cause a reduction in the potential dark toxicity.

Photothermal conversion efficiency and thermal stability

Nanoprecipitation of **NDNT** with 1,2-distearoyl-*sn-glycero*-3-phosphoethanolamine-*N*-[amino(polyethylene glycol)-$_{2000}$] (DSPE-PEG-$_{2000}$) was used to improve the water dispersity of **NDNT** because it is almost insoluble in water. To characterize the morphology of the nanoparticles, dynamic light scattering (DLS) and transmission electronic microscope (TEM) show that the NPs have well-defined spherical nanostructures, and the average diameter distribution is approximately 14 to 90 nm, which is appropriate for enhanced permeability and retention (EPR) *in vivo*. In order to achieve deep tissue penetration in the near infrared region (NIR) window, **NDNT** NPs were used in the subsequent experiments.

High photothermal conversion efficiency guarantees high photothermal therapy efficacy. To calculate the photothermal conversion efficiency, the temperature change was recorded. As shown in Fig. 2C, with laser irradiation, the temperature elevation of **NDNT** NPs is 25.8 °C, which is much higher than that of water under the same condition (4.6 °C). The photothermal conversion efficiency of **NDNT** NPs was calculated to be as high as 40.6%, promising the excellent phototherapy efficiency of such NPs. The cyclic thermal stability was estimated for 5 times, which is shown in Fig. 2D. It can be found that there is no obvious decay, suggesting the outstanding thermal stability of these NPs.

Cellular uptake, ROS generation and MTT assay *in vitro*

The cellular uptake of **NDNT** NPs in Du145 cells was investigated. As shown in Fig. 3A–D, **NDNT** NPs can be uptaken by
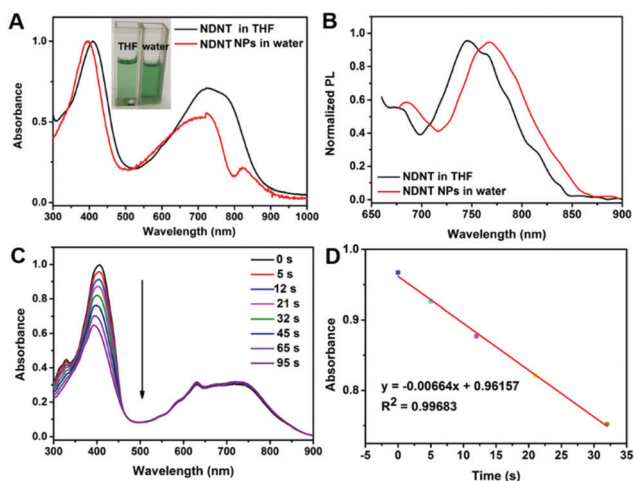

Fig. 1 (A) Normalized absorbance of **NDNT** in THF and NPs in water; (B) normalized PL of **NDNT** in THF and NPs in water; (C) degradation of DPBF under the presence of **NDNT** in DCM with laser irradiation; (D) linear fitting of the degradation of DPBF.
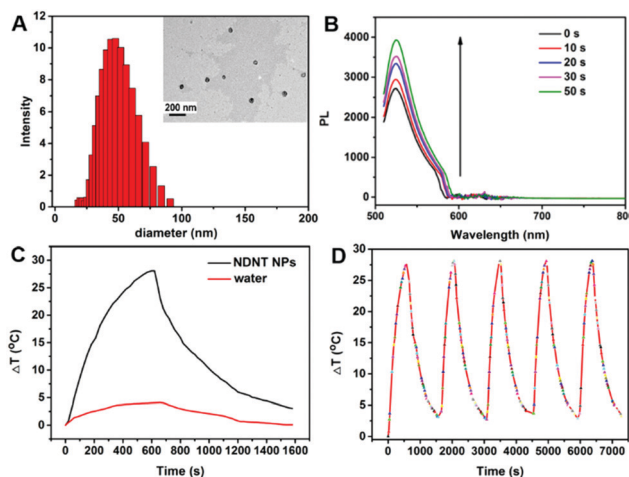

Fig. 2 (A) TEM and DLS of **NDNT** NPs in water; (B) PL of SOSG with irradiation; (C) heating and cooling curve of **NDNT** NPs with or without laser irradiation (730 nm, 1 W cm^{-2}); (D) thermal stability of **NDNT** NPs in water for 5 cycles.
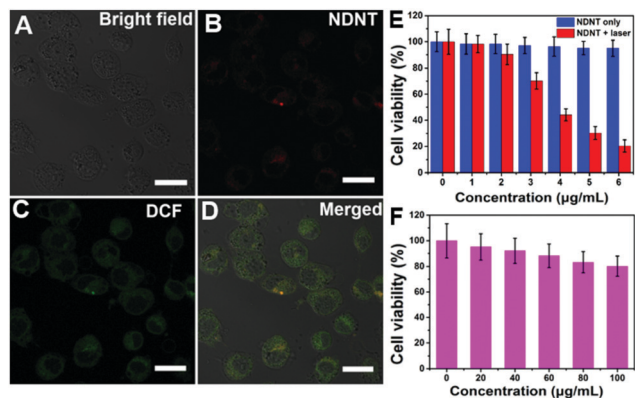
Fig. 3 (A–D) Cellular uptake and ROS generation of **NDNT** NPs with DCF as a probe in Du145 cells, scale bar: 10 µm; (E) MTT assay of **NDNT** NPs with different concentration with or without laser irradiation; (F) cell viability of **NDNT** NPs at high concentrations without irradiation.

Du145 cells and can generate ROS with DCF as a probe under light irradiation. To investigate the synergistic phototherapeutic effects of the **NDNT** NPs, we evaluated the inhibitory effect of **NDNT** NPs on the cell viability of human prostate cells (Du145) at different concentrations. After the treatment of **NDNT** NPs for 24 h, the MTT assay shows that the IC_{50} value is as low as 3.8 µg mL^{-1} (Fig. 3E). In addition, the group incubated with the nanoparticles without irradiation demonstrated a low dark toxicity. To further investigate the potential dark toxicity of the NPs, **NDNT** NPs were incubated with Du145 at high concentration (Fig. 3F). As a result, the cell viability remains high, showing the suitability of the NPs for PDT/PTT synergistic therapy.

In vivo photothermal imaging guided phototherapy

To further investigate the PDT and PTT synergistic therapeutic efficacy of **NDNT** NPs *in vivo*, 15 nude mice bearing the Du145
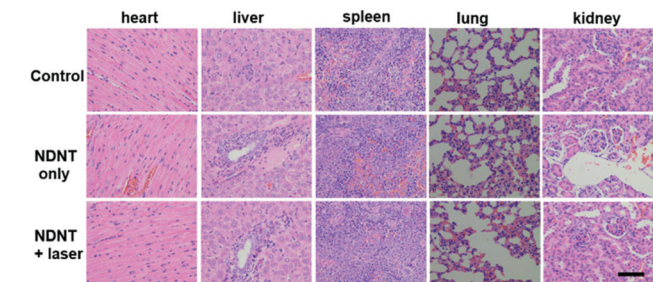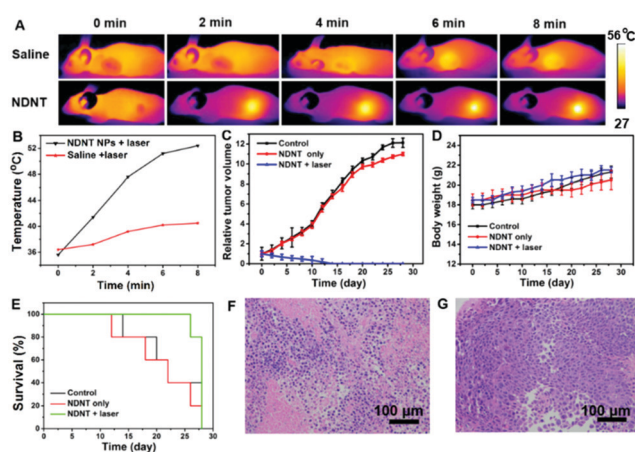

Fig. 4 (A) Photothermal imaging of control and **NDNT** groups with laser irradiation; (B) temperature elevation of control and **NDNT** group with irradiation for 2, 4, 6 and 8 min; (C) relative tumor volume of nude mice during treatment; (D) body weight of nude mice; (E) survival rate of nude mice during treatment; (F) H&E stained picture of the tumor of the control group; (G) H&E stained picture of the tumors in the **NDNT** only group. Scale bar: 100 µm.

Fig. 5 H&E stained pictures of normal tissues including the heart, liver, spleen, lung and kidney. Scale bar: 100 µm.

tumor were used in this study. As shown in Fig. 4A, under the irradiation for 8 min, a significant temperature elevation of approximately 18 °C was observed, compared with that of the control group (4.2 °C) (Fig. 4B). Fig. 4C shows that the tumor volume of both the control and the dark group increases at a high speed, while after the irradiation treatment, the tumor volume was greatly suppressed. The tumor of the illumination group completely disappeared even after six treatments, demonstrating the outstanding efficacy of the **NDNT** NPs. The mice were still alive for 16 days, no obvious recurrence was observed, indicates that **NDNT** NPs had high phototoxicity for the tumor treatment. Though the **NDNT** NPs inhibited the growth of tumor *in vivo*, their potential toxicity must still be comprehensively evaluated. During the treatment process, no significant difference between the body weight of mice in the three groups was observed (Fig. 4D), indicating the low dark toxicity of the **NDNT** NPs. The survival rate is shown in Fig. 4E.

After treatment, all the mice were sacrificed and the tumors were collected as well as the normal organs, including the heart, liver, spleen, lung, and kidney. According to the hematoxylin and eosin (H&E) stained images, we found no obvious changes in the normal organs between the control and the **NDNT** NPs treated groups (Fig. 4F and G). The results indicate that the **NDNT** NPs exerted anti-tumor activity without any adverse effects *in vivo*, suggesting their excellent bio-compatibility (Fig. 5).[31–36]

Conclusions

In summary, a heavy atom-free **NDNT** with a high $^1O_2$ QY of 55.2% was designed and prepared. The as-prepared NPs obtained by nanoprecipitation with DSPE-PEG$_{2000}$ still retained a high $^1O_2$ generation ability with SOSG as a probe, simultaneously providing a high photothermal conversion efficiency (40.6%), demonstrating the excellent phototherapy efficacy of such NPs. An *in vitro* MTT assay demonstrates that **NDNT** NPs with an ultralow IC_{50} of 3.8 µg mL^{-1} show a reasonably low dark toxicity even at a high concentration. *In vivo* photothermal imaging guided photo-therapy indicates that such NPs are able to inhibit the tumor growth in low doses while causing no damage to any normal tissue, suggesting the outstanding biosafety of such NPs. Our research therefore demonstrates the synthesis of a NIR heavy atom-free copolymer with high phototoxicity, low dark toxicity and good biocompatibility for imaging guided synergistic therapy.

Conflicts of interest

The authors declare no conflicts of interest.

Acknowledgements

Notes and references

1 R. L. Siegel, K. D. Miller and A. J. Dvm, *Ca-Cancer J. Clin.*, 2018, **68**, 7–30.

2 K. Ando, M. F. Heymann, V. Stresing, K. Mori, F. Redini and D. Heymann, *Cancer*, 2013, **5**, 591–616.

3 A. Matsunobu, R. Imai, T. Kamada, T. Imaizumi, H. Tsuji, H. Tsujii, Y. Shioyama, H. Honda, S. Tatezaki and W. G. B. S. T. Sarco, *Cancer*, 2012, **118**, 4555–4563.

4 D. Carrle and S. S. Bielack, *Int. Orthop.*, 2006, **30**, 445–451.

5 E. E. E. Santala, A. Rannikko and T. J. Murtola, *Int. J. Cancer*, 2019, **144**, 440–447.

6 A. Soldatov, C. A. J. von Klot, D. Walacides, T. Derlin, F. M. Bengel, T. L. Ross, H. J. Wester, K. Derlin, M. A. Kuczyk, H. Christiansen and C. Henkenberens, *Int. J. Radiat. Oncol., Biol., Phys.*, 2019, **103**, 1–5.

7 N. Shivran, M. Tyagi, S. Mula, P. Gupta, B. Saha, B. S. Patro and S. Chattopadhyay, *Eur. J. Med. Chem.*, 2016, **122**, 352–365.

8 M. Laine, N. A. Barbosa, A. Kochel, B. Osiecka, G. Szewczyk, T. Sarna, P. Ziółkowski, R. Wieczorek and A. Filarowski, *Sens. Actuators, B*, 2017, **238**, 548–555.

9 W. P. Fan, P. Huang and X. Y. Chen, *Chem. Soc. Rev.*, 2016, **45**, 6488–6519.

10 Z. J. Zhou, J. B. Song, L. M. Nie and X. Y. Chen, *Chem. Soc. Rev.*, 2016, **45**, 6597–6626.

11 A. Carija, N. Puizina-Ivic, D. Vukovic, L. Miric Kovacevic and V. Capkun, *Photodiagn. Photodyn. Ther.*, 2016, **16**, 60–65.

12 J. Yang, X. Q. Gu, W. T. Su, X. Y. Hao, Y. J. Shi, L. Y. Zhao, D. F. Zou, G. W. Yang, Q. Y. Li and J. H. Zou, *Mater. Chem. Front.*, 2018, **2**, 1842–1846.

13 L. Huang, Z. J. Li, Y. Zhao, J. Y. Yang, Y. C. Yang, A. I. Pendharkar, Y. W. Zhang, S. Kelmar, L. Y. Chen, W. T. Wu, J. Z. Zhao and G. Han, *Adv. Mater.*, 2017, **29**, 1604789.

14 G. W. Yang, X. Zhang, G. M. Li, J. Yang, L. Shen, D. Y. Chen, Q. Y. Li and D. F. Zou, *New J. Chem.*, 2018, **42**, 5395–5402.

15 Z. Yang, W. P. Fan, W. Tang, Z. Y. Shen, Y. L. Dai, J. B. Song, Z. T. Wang, Y. Liu, L. S. Lin, L. L. Shan, Y. J. Liu, O. Jacobson, P. F. Rong, W. Wang and X. Y. Chen, *Angew. Chem., Int. Ed.*, 2018, **57**, 14101–14105.

16 Z. F. Chang, L. M. Jing, B. Chen, M. S. Zhang, X. L. Cai, J. J. Liu, Y. C. Ye, X. D. Lou, Z. J. Zhao, B. Liu, J. L. Wang and B. Z. Tang, *Chem. Sci.*, 2016, **7**, 4527–4536.

17 H. He, S. S. Ji, Y. He, A. J. Zhu, Y. L. Zou, Y. B. Deng, H. T. Ke, H. Yang, Y. L. Zhao, Z. Q. Guo and H. B. Chen, *Adv. Mater.*, 2017, **29**, 1606690.

18 M. Li, Y. Gao, Y. Y. Yuan, Y. Z. Wu, Z. F. Song, B. Z. Tang, B. Liu and Q. C. Zheng, *ACS Nano*, 2017, **11**, 3922–3932.

19 X. L. Cai, C. J. Zhang, F. T. W. Lim, S. J. Chan, A. Bandla, C. K. Chuan, F. Hu, S. D. Xu, N. V. Thakor, L. D. Liao and B. Liu, *Small*, 2016, **12**, 6576–6585.

20 Y. J. Liu, P. Bhattarai, Z. F. Dai and X. Y. Chen, *Chem. Soc. Rev.*, 2019, **48**, 2053–2108.

21 X. S. Li, D. Y. Lee, J. D. Huang and J. Yoon, *Angew. Chem., Int. Ed.*, 2018, **57**, 9885–9890.

22 V. Glembockyte, M. Frenette, C. Mottillo, A. M. Durantini, J. Gostick, V. Štrukil, T. Friščić and G. Cosa, *J. Am. Chem. Soc.*, 2018, **140**, 16882–16887.

23 W. Sun, S. Y. Li, B. Häupler, J. Liu, S. B. Jin, W. Steffen, U. S. Schubert, H. J. Butt, X. J. Liang and S. Wu, *Adv. Mater.*, 2017, **29**, 1603702.

24 Z. W. Wei, M. Wu, S. Y. Lan, J. Li, X. L. Zhang, D. Zhang, X. L. Liu and J. F. Liu, *Chem. Commun.*, 2018, **54**, 13599–13602.

25 W. Zheng, G. Yang, S. T. Jiang, N. N. Shao, G. Q. Yin, L. Xu, X. P. Li, G. S. Chen and H. B. Yang, *Mater. Chem. Front.*, 2017, **1**, 1823–1828.

26 W. Sun, M. Parowatkin, W. Steffen, H. J. Butt, V. Mailänder and S. Wu, *Adv. Healthcare Mater.*, 2016, **5**, 467–473.

27 M. Yamaguchi, S. Ito, A. Hirose, K. Tanaka and Y. Chujo, *Mater. Chem. Front.*, 2017, **1**, 1573–1579.

28 B. Wei, M. Y. Guo, Y. M. Lu, P. P. Sun, G. W. Yang and Q. Y. Li, *Z. Anorg. Allg. Chem.*, 2018, **644**, 6–11.

29 Z. Y. Fan, D. D. Li, X. Yu, Y. P. Zhang, Y. Cai, J. J. Jin and J. H. Yu, *Chem. – Eur. J.*, 2016, **22**, 3681–3685.

30 E. Secret, M. Maynadier, A. Gallud, A. Chaix, E. Bouffard, M. Gary-Bobo, N. Marcotte, O. Mongin, K. El Cheikh, V. Hugues, M. Auffan, C. Frochot, A. Morere, P. Maillard, M. Blanchard-Desce, M. J. Sailor, M. Garcia, J. O. Durand and F. Cunin, *Adv. Mater.*, 2014, **26**, 7643–7648.

31 G. Song, J. Hao, C. Liang, T. Liu, M. Gao, L. Cheng, J. Hu and Z. Liu, *Angew. Chem., Int. Ed.*, 2016, **55**, 2122–2126.

32 C. R. Gordijo, A. Z. Abbasi, M. Ali Amini, H. Y. Lip, A. Maeda, P. Cai, P. J. O'Brien, R. S. DaCosta, A. M. Rauth and X. Y. Wu, *Adv. Funct. Mater.*, 2015, **25**, 1858–1872.

33 Z. Yang, R. Tian, J. Wu, Q. L. Fan, B. C. Yung, G. Niu, O. Jacobson, Z. T. Wang, G. Liu, G. Yu, W. Huang, J. B. Song and X. Y. Chen, *ACS Nano*, 2017, **11**, 4247–4255.

34 Z. Yang, Y. L. Dai, C. Yin, Q. L. Fan, W. Zhang, J. B. Song, G. C. Yu, W. Tang, W. P. Fan, B. C. Yung, J. Li, X. Li, X. Li, Y. Tang, W. Huang, J. B. Song and X. Y. Chen, *Adv. Mater.*, 2018, **30**, 1707509.

35 Z. Yang, J. B. Song, W. Tang, W. P. Fan, Y. L. Dai, Z. Y. Shen, L. S. Lin, S. Cheng, Y. Liu, G. Niu, P. Rong, W. Wang and X. Y. Chen, *Theranostics*, 2019, **9**, 526.

36 Z. Yang, Y. L. Dai, L. Shan, Z. Y. Shen, Z. T. Wang, B. C. Yung, O. Jacobson, Y. Liu, W. Tang, S. Wang, L. S. Lin, G. Niu, P. Huang and X. Y. Chen, *Nanoscale Horiz.*, 2019, **4**, 426–433.

This journal is © The Royal Society of Chemistry and the Chinese Chemical Society 2019

Mater. Chem. Front., 2019, **3**, 1123–1127 | 1127